Improvement of Radiotracer Residence Time Distribution Analysis in Industrial Applications

H. Kasban, Elsayed H. Ali, Mohamed S. EL-Tokhy and H. Arafa
Department of Engineering, Nuclear Research Centre, Egyptian Atomic Energy Authority, P. No 13759, Inshas, Egypt

Key words: Radiotracer, residence time distributions, axial dispersion flow model, tanks in series flow model

Corresponding Author:
Elsayed H. Ali
Department of Engineering, Nuclear Research Centre, Egyptian Atomic Energy Authority, P. No 13759, Inshas, Egypt

Abstract: This study is concerned with the characterization and assessment of Residence Time Distribution (RTD) using signal processing algorithms. Besides, implicit and explicit models of the RTD signals are proposed. The experimental system of captured signals includes ^{99}Mo radiotracer, scintillator detector and DAS. Various algorithms are implemented for the analysis of the acquired signal. These algorithms are baseline restoration, background correction, statistical error computation, radioactive decay correction, signal de-noising and dead time correction methods. A quantitative and qualitative measure of the proposed algorithms is conducted. Analytical treatment of RTD is investigated that validated through comparison with introduced block diagram models by MATLAB Simulink environment. Additionally, the activity of used radiotracer activity is experimentally measured using Axial Dispersion Flow Model (ADFM) and Tanks in Series Flow Model (TSFM). The total amount of calculated tracer output is found to be of 112018 CPS. The proposed algorithms are observed to achieve a notable precision in the analysis of radiotracer applications.

INTRODUCTION

RTD considered an important tool for analysis of industrial units and reactors. The RTD of fluid flow in process equipment determines their performance[1-4]. RTD is the most informative characteristics to obtain hydrodynamic information. It is a particularly important parameter in industrial applications. The interpretation of the RTD curves helps in diagnostics and the characterization of a mixing process[5, 6]. The RTD is applicable across a broad industrial spectrum such as petroleum, petrochemical industries, and mineral processing. Moreover, the wastewater treatment sectors are identified as the most appropriate target beneficiaries of radioisotope applications[7]. In other words, the RTD is a Probability Density Function (PDF) that may be characterized using statistical moments. Therefore, it is a PDF that describes the amount of time that fluid elements spend inside the reactor[8-10]. The RTD and the actual Mean Residence Time (MRT) estimations from theoretical relationships are complex due to three components, mass transport characteristics and segregation affecting solid holdup. Therefore, the experimental RTD determination is suitable for industrial applications. The RTD was measured using the radioactive tracer technique. This technique allows for non-invasive radiotracer detection for characterizing the solid and liquid mixing regimes without disturbances[5]. The experimental RTD data analysis provides valuable information about the fluid flow behavior, the degree of
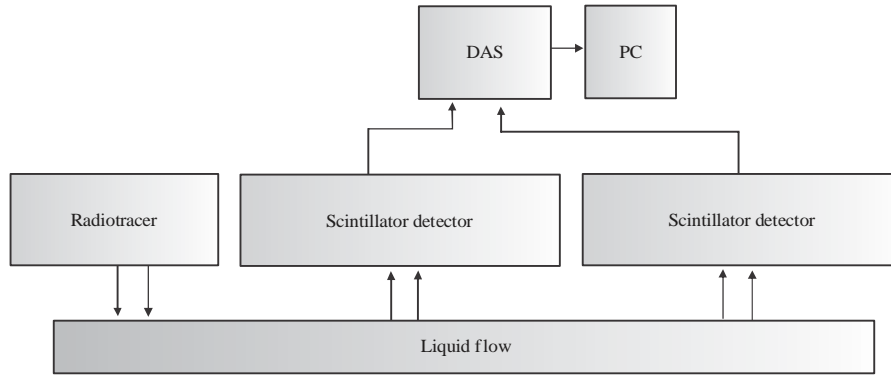
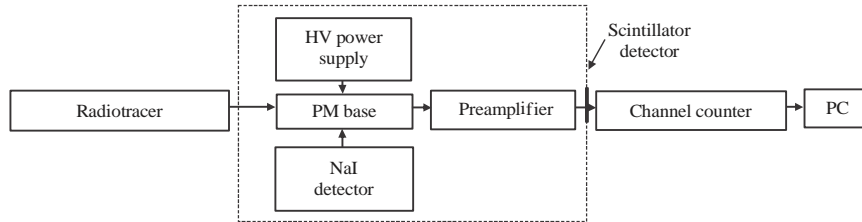Fig. 1: Experimental setup of RTD measured signal

Fig. 2: Block diagram for RTD signal measurements

radial and axial dispersion and possible flow problems in the exchanger such as stagnation or short-circulating. Radiotracer injections can be considered a good choice for obtaining the RTD in industrial processing vessels and wastewater treatment systems. Therefore, it is important to measure and obtain the RTD curve complemented with the temperature profile measurements used to assess the influence of the operating conditions on the fluid flow behavior[11, 12].

Several empirical models have been used in RTD studies. These empirical models involve interconnected perfectly mixed and plug flow sub reactors of unequal volume arranged in series and parallel[10]. The theoretical model solutions have poor convergence properties. Moreover, these are too complicated. Therefore, MATLAB Simulink is used for modeling of RTD. Consequently, four-block diagram models are proposed. These models are ADFM, perfect mixers in the series model, perfect mixers in the series exchange model and perfect mixers in the parallel model. These models are fitted to the RTD signal that obtained from real measurements. Moreover, this study aims to present models that enable to predicting the RTD under the effect of various parameters. The advantages of these models are simplicity and accurate results in compared with other empirical software[10].

The RTD system's experimental setup consists of more than one scintillator detector, data acquisition system (DAS), coaxial cables, and laptop for signal recording and analysis. The DAS collects the acquired radiation signal through computer software. Then, signal processing on the digitized signal is performed. Radiotracer signal analysis and recognition still represent challenges in industrial and environmental applications, especially in RTD measurement[2, 4, 9]. Therefore, background correction and signal de-noising using different digital filters are one of the works. The theoretical study is another scope of this work using different simulation techniques such as SIMULINK environments. In other words, the experimental radiation signals are collected. Then, different algorithms for signal processing are prepared. MATLAB environment is employed for signal analysis. Other environments may is used for theoretical analysis, such as the Maple environment[9, 13, 14]. The obtained results are summarized and analyzed. The objective of this work is to study different algorithms for RTD signal treatments. Also, the explicit solution of RTD Models receives little attention in the literature (Fig. 1).

Experimental setup: In this system, the components of the system for signal processing algorithms are described. It contains the following elements; Molybdenum-99 (^{99}Mo) with activity 5 mCi, scintillator detector with NaI (TI), Ludlum DAS and Laptop. Figure 2 depicts the considered system block diagram for recording the RTD signal.

Handling of RTD radiation signal

Background correction: It is essential to consider this background of gamma at low activity measurements. Therefore, we applied two different methods on the acquired RTD signal. Here, we are interested in removing the existing background radiation by applying the following formula[5]:

$$Tm = \mu m - \xi m \tag{1}$$

Tm, μm, and ξm denote the background-corrected signal, original signal, and minimum value of the original signal. The ^{99}Mo radiation signal was measured. Then, the radiation source is moved away from the radiation detector and the detector is exposed to the free air. Subsequently, subtract the acquired background signal from the measured one according to the following relation:

$$T_s = \eta_s - \sigma_s \tag{2}$$

where Cs, ηs and σs denote the background corrected signal, acquired 60°C radiation signal and background signal, respectively.

Base line restoration of RTD signal: The corrected background RTD signal is shifted to be below the base line. However, it is important to restore the corrected signal to be above the x-axis line or the RTD signal's baseline. It is done by the following equation:

$$\Delta = \chi - \Psi \tag{3}$$

where, x and Ψ denote the background-corrected signal and minimum count in the background corrected signal, respectively.

RTD signal de-noising using complex wavelet transform: Here, the experimental components for studying and evaluation of noise elimination using Complex Wavelet Transform (CWT) algorithms are stated. It covers the following components; ^{99}Mo as a radiotracer, scintillation detector, amplifier, DAS and laptop. The scintillation detector is connected to amplifier through coaxial cable which in turn connected to the laptop. MATLAB environment is used to perform noise elimination using CWT evaluation. Therefore, an algorithm for signal de-noising using CWT is studied on the measured RTD radiation signals. This algorithm is proposed for multidimensional signal processing by Roshani *et al.*[15], Zniyed *et al.*[16]. Thus, an algorithm of noise elimination using CWT is illustrated in study. Moreover, different wavelet transform levels are considered. However, further details of CWT are illustrated in our previous research.

An algorithm of the CWT algorithm for noise elimination of RTD radiation signal:

- Use ^{99}Mo radiation source
- Signal detection by Scintillator detector
- Acquire the signal by data acquistion system
- Store the RTD signal on excel sheet on personal computer
- Determine total number of levels in the wavelet tree
- Applying the CWT to the input signal
- Applying the inverse CWT
- Obtain the reconstructed RTD radiation signal

Normalization of RTD radiation signal and moments computation: It is necessary to consider the tracer curve normalization area because it makes the computations of moments much simpler. The normalization curve is obtained by dividing each data point by the area under the curve[1, 2]:

$$E(t) = \frac{n_c(t)}{\int_0^\infty n_c(t)dt} \tag{4}$$

where $n_c(t)$ denotes the corrected count rate. However, one of the cores of RTD data treatment is the moment's computation. It is used to describe the RTD functions in statistical parameters such as MRT and Standard Deviation. It is defined by Pant *et al.*[4]:

$$T_i = \int_0^\infty t^i E(t) \tag{5}$$

On the other hand, the MRT is equivalent to the first moment.

The proposed RTD modeling: ADFM is a widespread one for practical applications. This flow is the superimposition of convection and some amount of dispersion[1, 2]. A Fickian law can express the dispersion in 1-D, tracer concentration C is given by the following balanced equation:

$$\frac{\partial C}{\partial t} + u\frac{\partial C}{\partial x} = D\frac{\partial^2 C}{\partial x^2} \tag{6}$$

where, U and D are, respectively, the fluid velocity and axial dispersion coefficient, this formula has no explicit solution. So, it is manipulated using the separation of the variable method. Thus, it is assumed that C(x,t) = X(x)T(t) (with X and T are a function of the fluid concentration). The derivatives of concentration for respect to axial movement and time are as follows:

$$C_x = \frac{\partial C}{\partial x} = \dot{X}(x)T(t) \qquad (7)$$

The second differentiation of the concentration with respect to axial flow is given by:

$$C_{xx} = \frac{\partial^2 C}{\partial x^2} = \ddot{X}(x)T(t) \qquad (8)$$

Additionally, the differentiation of concentration with respect to flow time is initiated by:

$$C_t = \frac{\partial C}{\partial t} = \dot{T}(t)X(x) \qquad (9)$$

The substitution from (Eq. 7-9) into (Eq. 6) yields:

$$X(x)\dot{T}(t) + u\dot{X}(t)T(t) = D\ddot{X}(x)T(t) \qquad (10)$$

By dividing both sides on X(x)T(t), we obtain:

$$\frac{\dot{T}(t)}{T(t)} + u\frac{\dot{X}(x)}{X(x)} = D\frac{\ddot{X}(x)}{X(x)} \qquad (11)$$

It is assumed that:

$$D\frac{\ddot{X}(x)}{X(x)} = \sigma$$

so, the previous formula is described by:

$$\ddot{X}(x) - \frac{\sigma}{D}X(x) = 0 \qquad (12)$$

Assume the solution of the above equation is given by (x) = e^r x. The substitution into (Eq. 12) yields:

$$\frac{\partial}{\partial x^2}e^{rx} - \frac{\sigma}{D}e^{rx} = 0 \text{ and } \left(r^2 - \frac{\sigma}{D}\right)e^{rx} = 0 \qquad (13)$$

where, $e^{rx} \neq 0$. So, $r^2 - \sigma/D = 0$ which means

$$r = \pm\sqrt{\frac{\sigma}{D}}$$

Therefore, the general solution of Eq. 12 is given by:

$$X(x) = d_1 e^{\left(\sqrt{\frac{\sigma}{D}}\right)x} + d_2 e^{\left(\sqrt{\frac{\sigma}{D}}\right)}x \qquad (14)$$

Similarly, Eq. 11 can be rewritten as:

$$\frac{\dot{T}(t)}{T(t)} + u\frac{\dot{X}(x)}{X(x)} = \sigma \qquad (15)$$

From (Eq. 12) and (Eq. 15), we get:

$$\frac{\dot{T}(t)}{T(t)} + u\frac{re^{rx}}{e^{rx}} = \sigma \qquad (16)$$

On other hand $\frac{\dot{T}(t)}{T(t)} + ur = \sigma$ simplified as:

$$\dot{T}(t) = (\sigma - ur)T(t) \qquad (17)$$

Assume the solution (Eq. 10) is given as T(t) e^{st}. Putting it into (Eq. 17) yields $se^{st} = (\sigma - ur)e^{st}$ s = σ-ur. Therefore, $s = \sigma \pm \sqrt{\frac{\sigma}{D}}u$ the solution (Eq. 17) is given by:

$$T(t) = d_3 e^{\left(\sigma + \sqrt{\frac{\sigma}{D}}\right)t} + d_4 e^{\left(\sigma - \sqrt{\frac{\sigma}{D}}\right)t} \qquad (18)$$

The substitution from (Eq. 18) and (14) into C (x, t) = X(x)T (t) yields:

$$C(x,t) = \left[d_1 e^{\left(\sqrt{\frac{\sigma}{D}}\right)x} + d_2 e^{-\left(\sqrt{\frac{\sigma}{D}}\right)x}\right]\left[d_3 e^{\left(\sigma + \sqrt{\frac{\sigma}{D}}\right)t} + d_4 e^{\left(\sigma - \sqrt{\frac{\sigma}{D}}\right)t}\right] \qquad (19)$$

The arbitrary constants d_1 to d_4 are deduced using the next boundary conditions that stated as:

$$C(0,0) = 0 \qquad (20)$$

$$C(l,t) = E \qquad (21)$$

Therefore, putting (Eq. 20) in (Eq. 19), we get:

$$0 = (d_1 + d_2)(d_3 + d_4) \qquad (22)$$

Also, the substitution from Eq. (21) in Eq. (19), we obtain:

$$E = \left[d_1 e^{\left(\sqrt{\frac{\sigma}{D}}\right)l} + d_2 e^{-\left(\sqrt{\frac{\sigma}{D}}\right)l}\right]\left[d_3 e^{\left(\sigma + \sqrt{\frac{\sigma}{D}}\right)t} + d_4 e^{\left(\sigma - \sqrt{\frac{\sigma}{D}}\right)t}\right] \qquad (23)$$

In addition, if X (0) = 0 it yields $d_1 + d_2 = 0$:

$$d_1 = -d_2 \qquad (24)$$

If X (l) = 0 in Eq. 14, we obtain:

$$0 = d_1 e^{\left(\sqrt{\frac{\sigma}{D}}\right)l} + d_2 e^{\left(\sqrt{\frac{\sigma}{D}}\right)l} \qquad (25)$$

By manipulating (Eq. 24) and (Eq. 25), we get:

$$d_1 e^{\left(\sqrt{\frac{\sigma}{D}}\right)l} - d_1 e^{-\left(\sqrt{\frac{\sigma}{D}}\right)l} = 0 \qquad (26)$$

With assuming $l \neq 0$ in (Eq. 26), we get:

$$e^{\left(\sqrt{\frac{\sigma}{D}}\right)l} = e^{-\left(\sqrt{\frac{\sigma}{D}}\right)l} \qquad (27)$$

From (Eq. 27), we obtain:

$$e^{2\left(\sqrt{\frac{\sigma}{D}}\right)l} = 1 \qquad (28)$$

Take natural logarithmic for both sides in (Eq. 28) we obtain:

$$2\left(\sqrt{\frac{\sigma}{D}}\right)l = 0 \qquad (29)$$

Using euler expression $e^{-i\theta} = \cos\theta + i\sin\varphi$, Eq. (29) can be rewritten as:

$$2\left(\sqrt{\frac{\sigma}{D}}\right)l = 2\pi ki \qquad (30)$$

Therefore, the previous formula can be expressed as:

$$\sigma = \frac{-\pi^2 k^2}{l^2} D \qquad (31)$$

From (Eq. 18), we get T (0) = 0:

$$d_3 + d_4 = 0 \qquad (32)$$

From (Eq. 19, 31 and 32), we obtain:

$$C(x,t) = d_1 d_3 \left[e^{\left(\sqrt{\frac{\sigma}{D}}\right)l} - e^{-\left(\sqrt{\frac{\sigma}{D}}\right)l} \right]\left[e^{\left(\sigma + \sqrt{\frac{\sigma}{D}}\right)t} - e^{-\left(\sigma - \sqrt{\frac{\sigma}{D}}\right)t} \right] \qquad (33)$$

The substitution from (Eq. 31) into Eq. (33), we arrived to:

$$C(x,t) = d_1 d_3 \left[e^{\left(\sqrt{\frac{-\pi^2 k^2}{l^2}D}{D}\right)x} - e^{-\left(\sqrt{\frac{-\pi^2 k^2}{l^2}D}{D}\right)x} \right]\left[e^{\left(\frac{-\pi^2 k^2}{l^2}D + \sqrt{\frac{-\pi^2 k^2}{l^2}D}{D}\right)t} - e^{-\left(\frac{-\pi^2 k^2}{l^2}D - \sqrt{\frac{-\pi^2 k^2}{l^2}D}{D}\right)t} \right] \qquad (34)$$

For simplicity, it is assumed that $\sqrt{-1} = i$. So, Eq. (34) is simplified to be:

$$C(x,t) = d_1 d_3 \left[e^{\frac{\pi ki}{1}x} - e^{-\frac{\pi ki}{1}x} \right]\left[e^{\left(\frac{-\pi^2 k^2}{l^2}D + \frac{\pi ki}{1}\right)t} - e^{-\left(\frac{-\pi^2 k^2}{l^2}D - \frac{\pi ki}{1}\right)t} \right] \qquad (35)$$

After some mathematical treatments for Eq. 35, we get:

$$C(x,t) = -(d_1 d_3)(4) e^{\left(\frac{-\pi^2 k^2}{l^2}D\right)t} \sin\left(\frac{\pi k}{l}x\right) * \sin\left(\frac{\pi k}{l}t\right) \qquad (36)$$

The perfect mixer model has been extensively used to characterize and simulate grinding processes. This is due to its simple conceptual representation and suitable mathematical treatment[3, 15]. Here, two different mathematical models are introduced. The first model depends on the analytic solution of the model differential equation. The perfect mixers in the series model are composed of perfect mixing tanks connected in series as shown in Fig. 3. This model can be described by Charlton and Wellman[1] and Korchi et al.[2]:

$$\frac{dC}{dt} = \frac{JQ}{V}\left(C_p - C\right) \qquad (37)$$

where, J, Q, V, C_p denote the number of mixers, flow rate, tank volume and previous concentration in the tank, respectively. The solution of the previous equation represents the tracer at the system output. The solution of Eq. 17 is based on the Laplace transform. Therefore, the Laplace transform method was applied. Then, the following equation as a function in s-domain is stated as:

$$C = \frac{QJC_p}{s(Vs + QJ)} \qquad (38)$$

Then, inverse Laplace is applied that leads to the following RTD function in the time domain:

$$C = 2C_p e^{\frac{QJt}{2V}} \sinh\left(\frac{QJt}{2V}\right) \qquad (39)$$

However, the second proposed solution depends on the general integration mathematical solution. This solution leads to the following radiation concentration in the time domain at the system output:

$$C = C_p\left(1 - e^{\frac{QJt}{V}}\right) \qquad (40)$$

This equation describes the radiotracer at the output of the system. However, an implicit solution describing
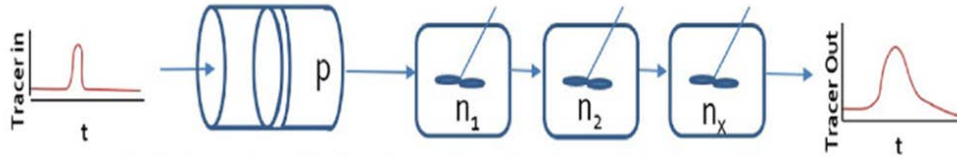
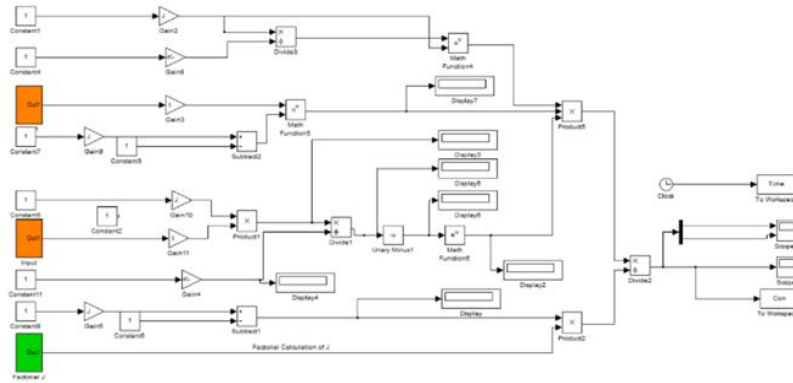Fig. 3: Perfect mixers in the series method

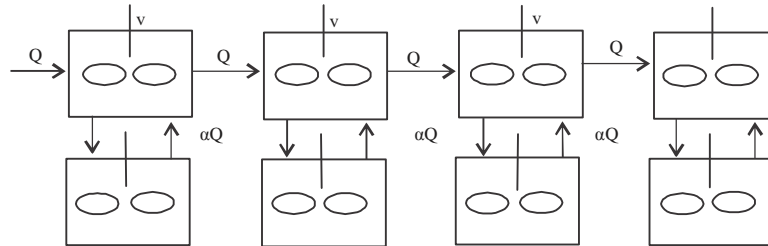Fig. 4: The proposed block diagram model of perfect mixers in series model

Fig. 5: Perfect mixers in service with exchange

the RTD at the output of the system is introduced. This solution depends on MATLAB Simulink. Therefore, a block diagram model for perfect mixers in series is introduced, as shown in Fig. 4. This model has the advantage of its simplicity and can be compared to the RTD Software that provided by IAEA Software.

The perfect mixers models in series with the exchange are used in the simulation of industrial applications. The representation of this model is shown in Fig. 5. The age, α, of a fluid at a time, t, represents the difference between this time and the time at the beginning of injection[1, 2]. This model is described by:

$$\frac{dC}{dt} = \frac{JQ}{V}\left[\left(C_p\text{-}C\right)+\alpha\left(C^2\text{-}C\right)\right] \tag{41}$$

The solution of this model equation is introduced using two different analytic techniques. The first solution depends on the Laplace transform. Thus, the tracer concentration, as a function in the s-domain is introduced:

$$C(s) = \frac{QJC_p\left(1+\alpha C_p\right)}{s\left(Vs+QJ+\alpha QJ\right)} \tag{42}$$

Then, the radiotracer concentration as a function of time domain is deduced by taking inverse Laplace transform:

$$C = \frac{2C_p\left(1+\alpha C_p\right)}{1+\alpha}e^{-\frac{QJ(1+\alpha)t}{2V}}\sinh\left(\frac{QJ(1+\alpha)t}{2V}\right) \tag{43}$$
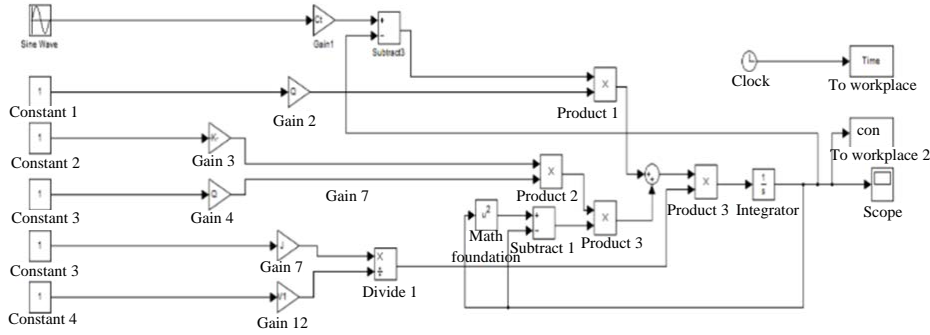
Fig. 6: The proposed block diagram model of perfect mixers in series exchange
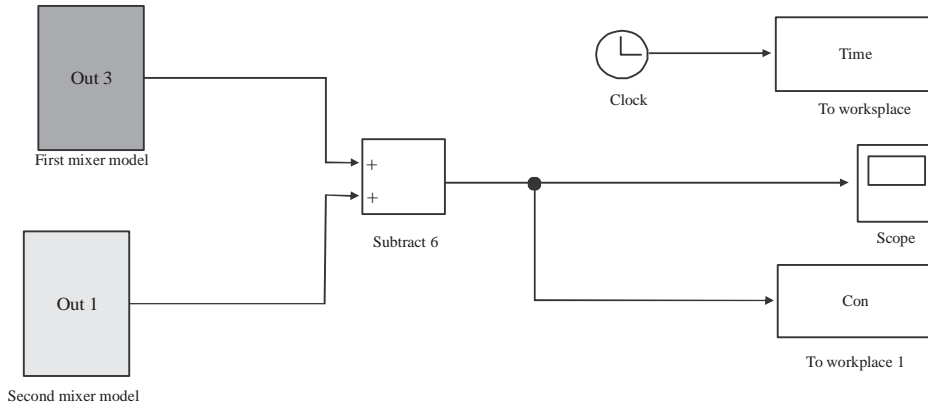

Fig. 7: The proposed block diagram model of perfect mixers in parallel model

The second solution is based on general mathematical integration. Consequently, the radiotracer concentration at the output of the system is given by:

$$C = \frac{C_p\left(1+\alpha C_p\right)}{1+\alpha}\left(1-e^{-\frac{QJ(1+\alpha)t}{V}}\right) \qquad (44)$$

Furthermore, a block diagram model through MATLAB Simulink is realized as depicted in Fig. 6. Here, the perfect mixer model in parallel is of primary concern. The equation of this model is described by:

$$C(t) = \frac{Q_1}{Q}\left(\frac{J}{\tau}\right)^J \frac{t^{J-1}e^{-\frac{Jt}{\tau}}}{(1-J)!} + \frac{Q-Q_1}{Q}\left(\frac{J_2}{\tau_2}\right)^J \frac{t^{J_2-1}e^{-\frac{J_2 t}{\tau}}}{(1-J_2)!} \qquad (45)$$

This equation can be modified and rewritten as:

$$C(t) = \frac{Q_1}{Q}\left(\frac{J}{\tau}\right)^J \frac{t^{J-1}e^{-\frac{Jt}{\tau}}}{(1-J)J!} + \frac{Q-Q_1}{Q}\left(\frac{J_2}{\tau_2}\right)^J \frac{t^{J_2-1}e^{-\frac{J_2 t}{\tau}}}{(1-J_2)J_2!} \qquad (46)$$

The proposed block diagram model for perfect mixers in parallel is illustrated in Fig. 7.

Activity estimation of measured RTD signal based on different flow model: In continuous flow measurements, the measured concentration of radiotracer depends on the flow model's internal dynamics. This means that a preliminary model must be selected based on the process of consideration[1,2]. ADFM and tank-in-series models are two simple and commonly used models to characterize the flow behaviour in industrial and hydrological systems[1, 2, 5, 11]. The activity of the tracer is obtained at $t = \tau$ and is given as:

$$A = 2C_{max} V \frac{\sqrt{\pi}}{\sqrt{P_e}} \qquad (47)$$

where, C_{max}, V, and pe denote maximum concentration (peak value) of tracer, the reactor's volume, and peclet number, respectively. Since the tank in the series model is accounted for high dispersion flows. Since, the tank in series model is accounted for high dispersion flows. The activity of tracer is obtained at $t = \tau$ ($\theta = 1$) and is given as Mishra and Singh[12]:
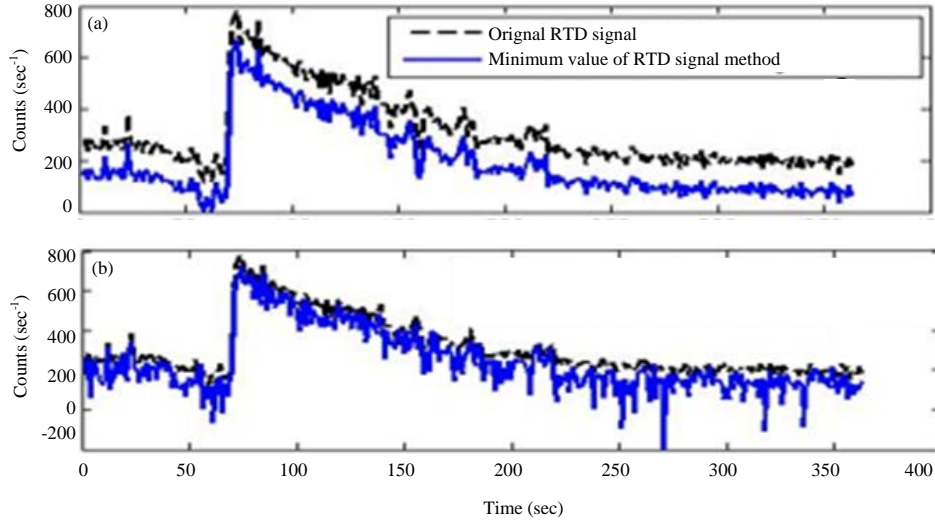
Fig. 8 (a, b): (a) Background corrected methods using and (b) Minimum value of the RTD signal method background subtraction method

$$A = C_{max} V \frac{(J-1)!}{J^J} e^J \qquad (48)$$

where, J denotes number of mixers. The MRT of fluid entering a perfectly mixed tank is given by the equation:

$$\tau = \frac{V}{Q} \qquad (49)$$

where, Q denotes the volumetric flow rate, and V is the volume. However, the real MRT can be experimentally determined from the measured RTD curve above. Consequently, the flow rate is determined by Eq. 50 (Fig. 9):

$$Q = \frac{V}{\tau}$$

RESULTS AND DISCUSSION

Two different methods are used for background correction of the acquired RTD radiation signal. These methods are the minimum value of the radiation signal method and subtraction method. The result of the first method is shown in Fig. 8a. The obtained result confirms that 115 counts per seconds of the minimum value of the original RTD signal were discovered (Table 1).

The result of the second method is depicted in Fig. 8b. However, we concluded that the background subtraction method introduces better

Table 1: Quantitative evaluation of background correction methods

Statistical measurements and processing methods	PSNR	Error
Minimum value of RTD signal	6.9168	0.33768
Background subtraction method	9.2819	0.25719

Table 2: Statistical evaluation of base line restoration method of RTD signal

Statistical measurements method	PSNR	Error
Base line restoration of RTD signal	5.5095	0.25719

results. Therefore, it is more accurate than the minimum value method. Consequently, it represents the actual background signal. Since, the background is varied at every instance. Therefore, our work in this manuscript will continue using the subtraction method.

Moreover, a quantitative evaluation of the considered background correction methods is depicted in Table 1. The obtained results confirm the superiority of the background subtraction method over the minimum value for RTD measured signals. However, the obtained RTD signal lies below the baseline. Consequently, another pre-processing step is necessary.

The output of the previous step is the input of the current one. Therefore, the baseline restoration method was applied for the restoration of the RTD signal. This method was applied for the background subtraction method only, as illustrated in Fig. 9. The evaluation of this method is illustrated through statistical measurements in Table 2. Although, the minimum value of the RTD signal shows less efficient results. It does not need the baseline restoration (Table 3).
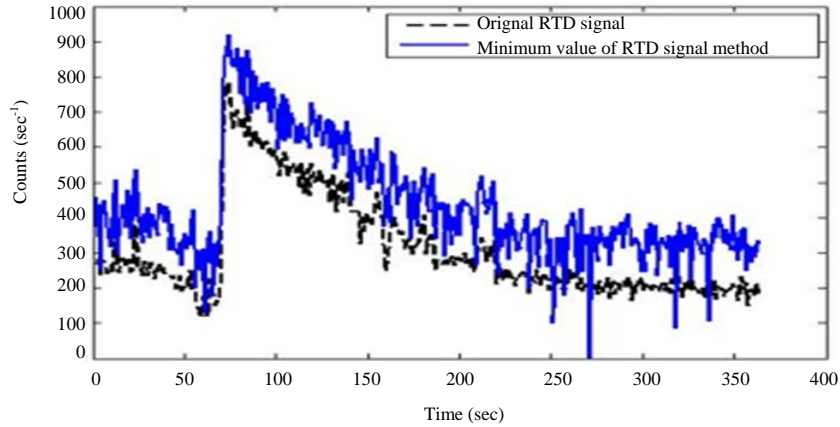
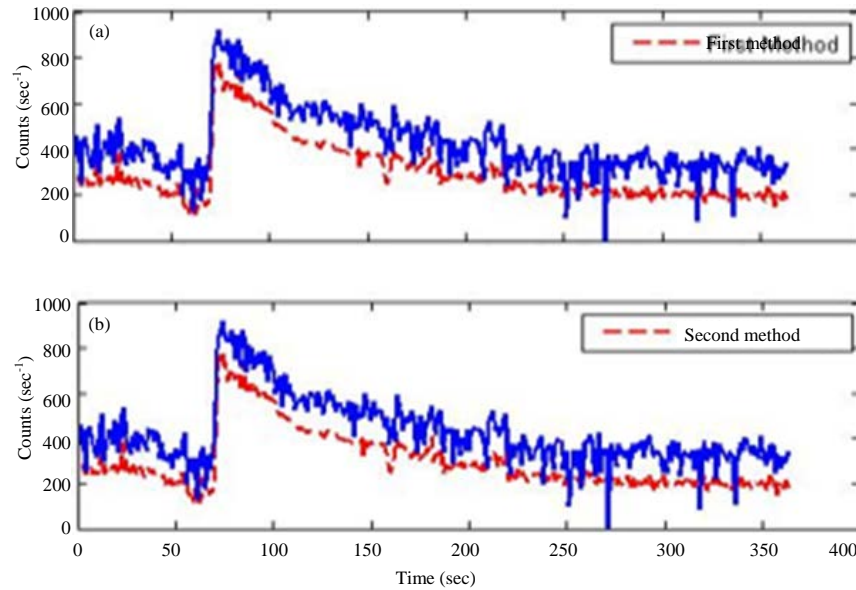Fig. 9: Baseline restoration of the background correction RTD signal by subtraction method

Fig. 10(a, b): Decay correction methods using (a) 1st Analytical method and (b) 2nd Analytical method

Table 3: Statistical parameters of acquired RTD radiation signal

Standard Deviation (σ)	SE (%)
159.9476	0.1018

Table 4: Statistical measurements of RTD signal de-noising using CWT

Statistics measurements	PSNR	Error	Executed time
Values	25.6244	0.1093	1.876806

It is essential to compute the statistical errors of the acquired RTD signal. These computations are based on analytical methodology. Therefore, the standard deviation and statistical error were computed as depicted in Table 3. There are two different analytical methods used for the correction of radioactive decay. These methods are depending on two different methods. The result of the first method is shown in Fig. 10a.

However, the result of the second method is depicted in Fig. 10b. Also, a comparison between these two methods is conducted, as depicted in Table 4. The obtained result confirms that the first analytical method introduces efficient results.

Here, a Low-Pass Filter (LPF) was applied. Therefore, apartial reconstruction of the original signal is introduced. Consequently, different levels of the filter bank were applied with the LPF to the acquired signal. The impulse response of the filters at different shifts is shown in Fig. 11. From this figure, the absolute value of the wavelet coefficients is obtained. Moreover, these filters are highly based around 0.0, 45, 90 and 135. Moreover, the real and complex parts of the complex filter constitute
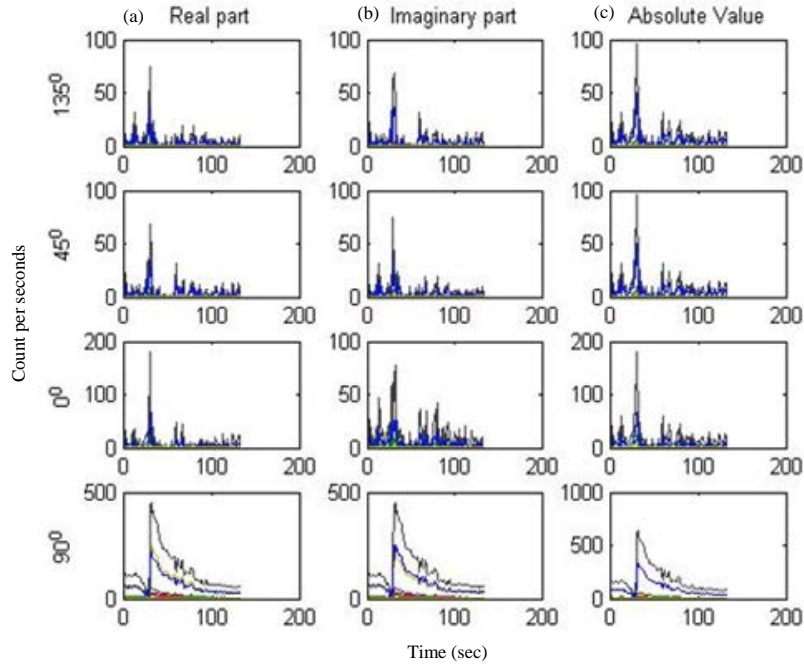
Fig. 11: The impulse response of the filters at different shifts with absolute value of the wavelet coefficient
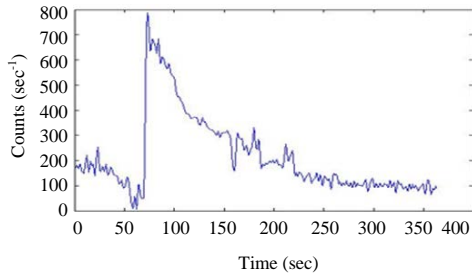

Fig. 12: Reconstructed signal using five levels of the algorithm
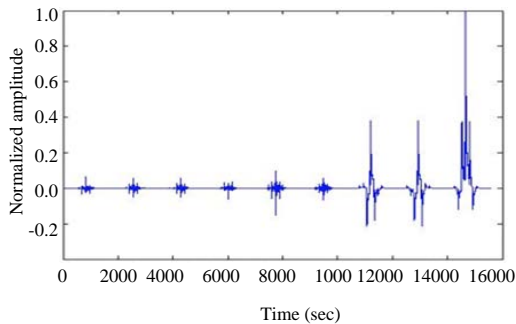

Fig. 13: Normalized amplitude of the RTD signal

Gabor-like filters as in. Furthermore, the RTD signal is reconstructed as shown in Fig. 12. From this figure, the transformed signals are shift-invariant.

Table 5: Statistical measurements of the obtained normalization curve

Statistics measurements	PSNR	Σ	Error
Values	6.9168	144.2526	0.33768

Table 6: Activity estimation of ADFM and TSFM

Reactor model	ADFM	TSFM
Activity (MBq)	0.1721	0.1230

Moreover, it is free of aliasing. Also, the normalized amplitude of level 1 CWT is depicted in Fig. 13. Statistical evaluation measurements consider the evaluation of the considered RTD signal de-noising algorithm as in Table 5.

The normalization of the area of the experimental tracer curve is depicted in Fig. 14. However, the statistical measurement of the normalized curve is illustrated in Table 6. From this table, the Standard Deviation is a measure for the broadening of the RTD. Moreover, moment computation is of primary concern. It is based on the probability of weighted moments and the coefficients of the shifted Legendre polynomial to calculate the first moments. The first-moment calculation is 193.5895. On the other hand, the MRT is equivalent to the first moment. Thus, the MRT with the RTD signal is shown in Fig. 15.

The radiotracer concentration with time at different mixers and MRT for perfect mixers in series is shown in Fig. 16-18, respectively. The concentration decreases with the number of mixers, as depicted in Fig. 16. Also, the radiotracer concentration
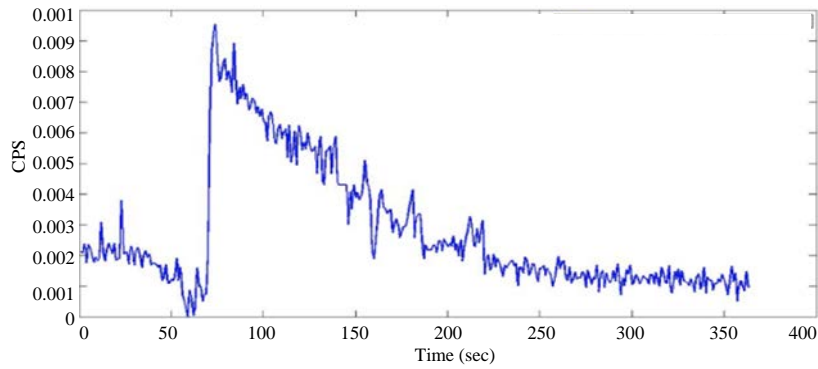
Fig. 14: Normalization of the area of experimental tracer curve
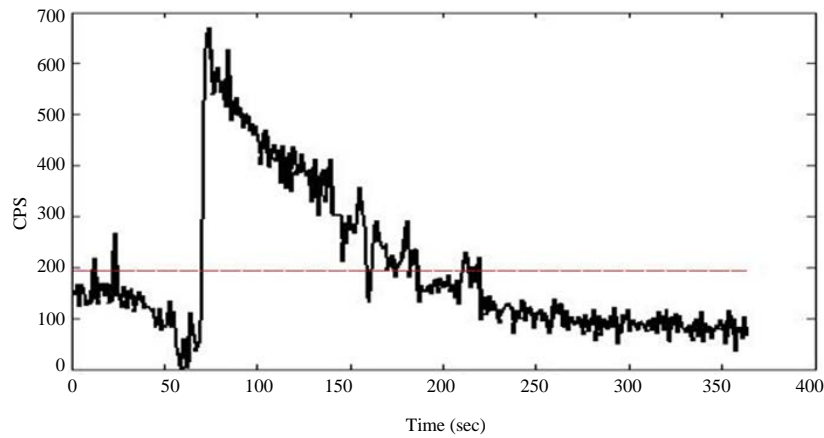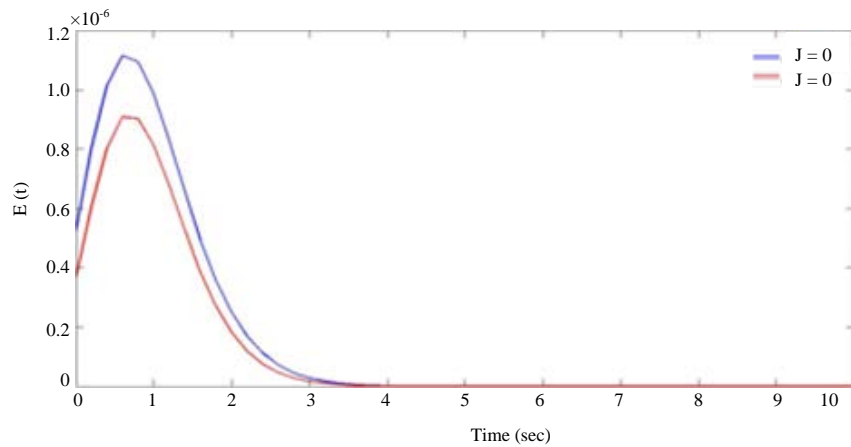

Fig. 15: MRT with RTD radiation signal

Fig. 16: The radiotracer concentration with time at different number of mixers with $\tau = 190$ sec

the radiotracer concentration decreases with MRT, as illustrated in Fig. 17. Figure 18 shows the relation between radiotracer concentration and time at different flow rates with J =1 0 and V = 1000 L. The results show that radiotracer moves fast by increasing

the flow rate. We noted that the radiotracer concentration at the outlet of the reactor is reaches a constant value or steady-state when the flow rate increased as we see from Fig. 19 the concentration remains constant at 30 seconds when flow rate Q is

11
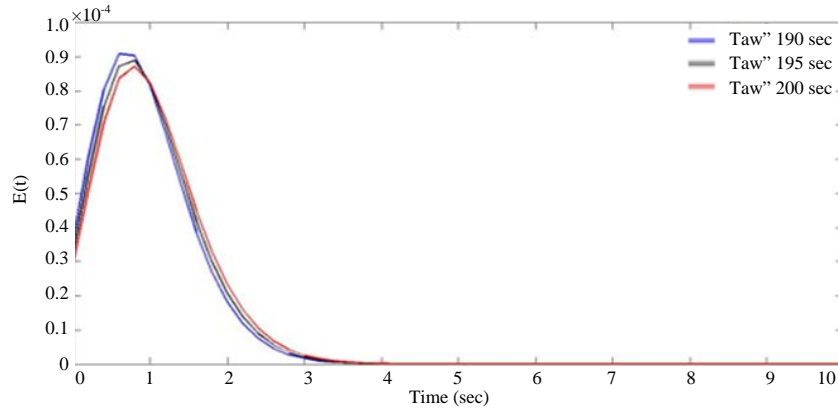
Fig. 17: The radiotracer concentration with time at different mean residence time with Pe = 9
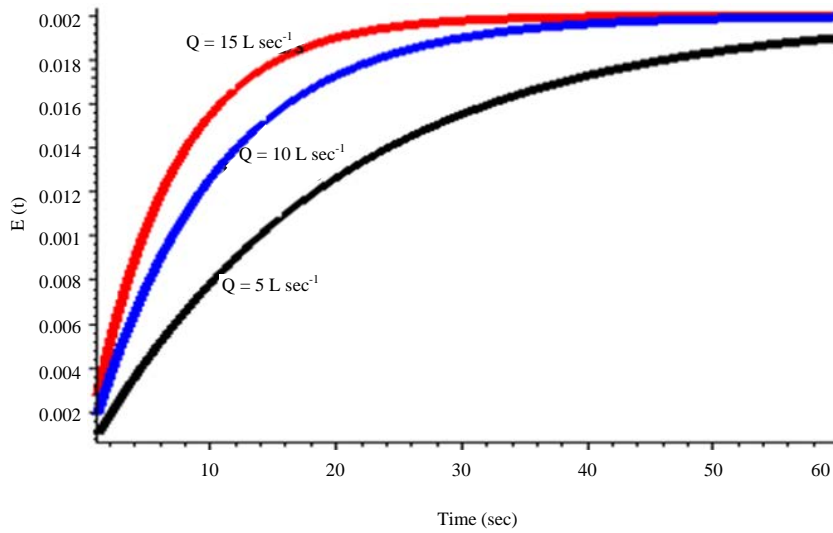
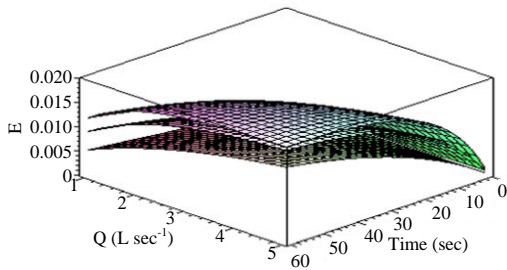Fig. 18: The radiotracer concentration with time at different flow rate with J = 10 and V = 1000L

Fig. 19: The radiotracer concentration with time and flow rate at different mixers numbers with V = 1000 L

15 L sec^{-1} while it takes 42 and 60 sec when the flow rate Q is 10 and 5 L sec^{-1}, respectively. For better illustration, the three-dimensional relation between radiotracer concentration with time at different flow rates with V = 1000 L is depicted in Fig. 19.

The activity of the tracer for ADFM and TSFM is computed. These calculations are shown in Table 6. Moreover, the tracer concentration at the outlet was found to be 112018 CPS.

The radiotracer concentration of perfect mixers in series exchange with time at different mixers, flow rate, tank volume and flow rate coefficient is depicted in Figs. 20-23, respectively. The radiotracer concentration measurement at the reactor's outlet does not change in shape with time with a number of mixers change, as shown in Fig. 20. However, the radiotracer concentration at the reactor's outlet is similar to increasing the flow rate as depicted in Fig. 21. Furthermore, the tank volume has an effect on tracer concentration at the outlet of the reactor. The radiotracer concentration decreases with increasing the tank volume, as in Fig. 22. Also, the radiotracer concentration decreases more time inside the tank by increasing the flow rate as in Fig. 23.

Moreover, the relation between radiotracer concentration and time at different first tank volume with
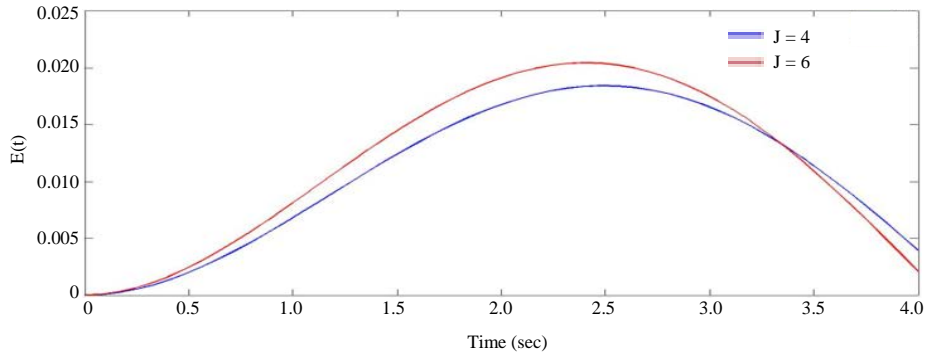
Fig. 20: The radiotracer concentration with time at different number of mixers with $V_1 = 175L$, $Q = 8.75L/s$ and $\alpha = 1$
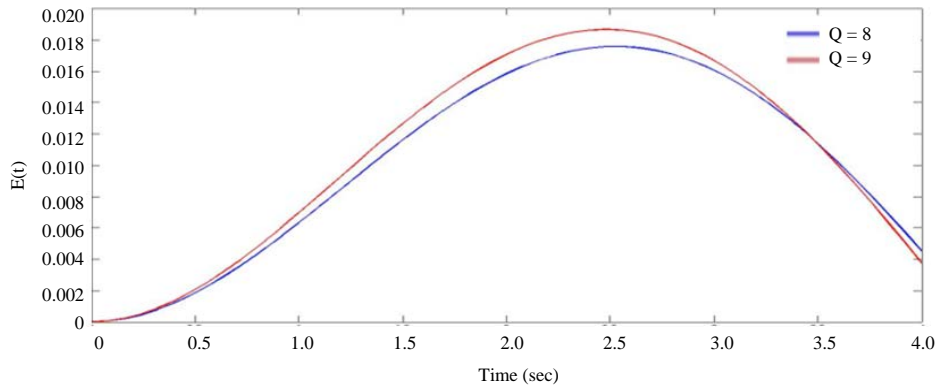

Fig. 21: The radiotracer concentration with time at different flow rates with $V_1 = 175L$, $J = 4$ and $\alpha = 1$
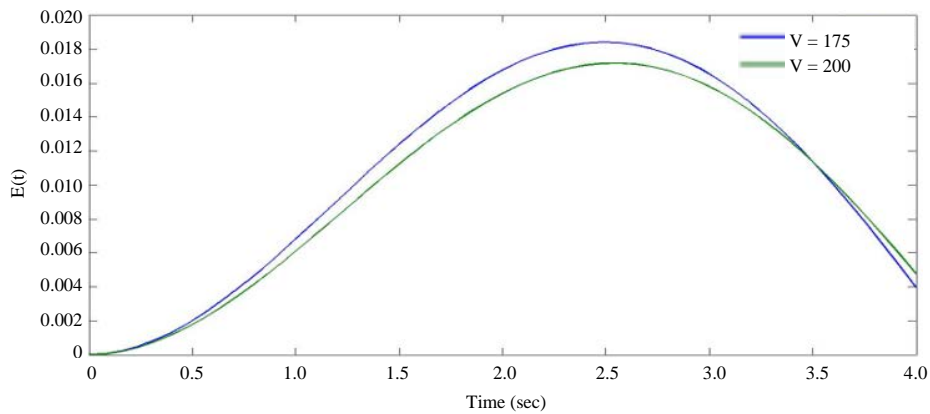

Fig. 22: The radiotracer concentration with time at different tank volumes with $J = 4$, $Q = 8.75L/s$ and $\alpha = 1$

$Q = 1L/s$ and $\alpha = 0.05$ is shown in Fig. 24. Furthermore, the radiotracer concentration with time and mixers numbers at different flow rates with $\alpha = 0.05$ is depicted in Fig. 25. The radiotracer concentration with time for perfect mixers in parallel at different mixers, MRT, flow rate, and flow rate in the first tank is depicted in Fig. 26-29, respectively. The radiotracer concentration profiles at the tank's outlet for the different number of mixers are similar but the radiotracer concentration is decreased with increasing the number of mixers, as shown in Fig. 26. However, the radiotracer concentration profile does not affect changing the MRT, as evident in Fig. 27. Moreover, the radiotracer concentration shape does not also affect the flow rate as in Fig. 28. The
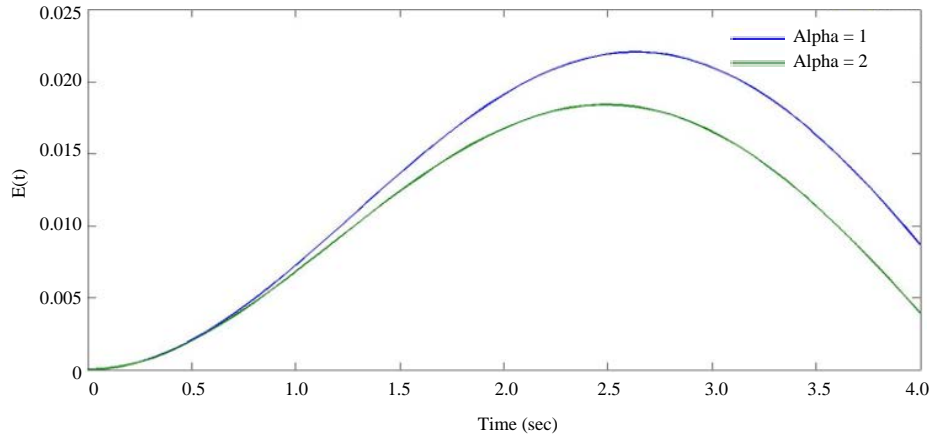
Fig. 23: The radiotracer concentration with time at different alpha with V1 = 175L, Q = 8.75L/s and V_1 = 175L

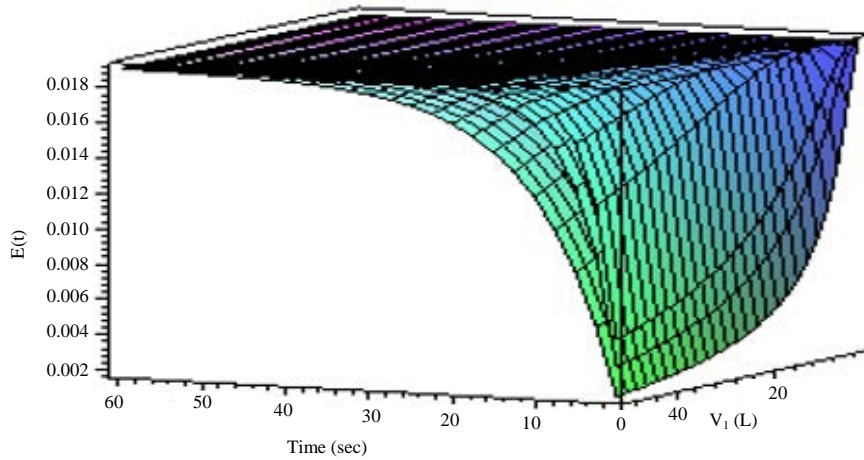Fig. 24: The radiotracer concentration with time at different first tank volume with Q = 1L/s and α = 0.05
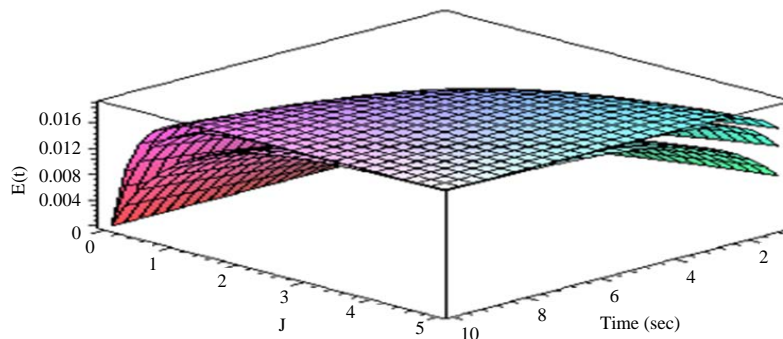

Fig. 25: The radiotracer concentration with time and mixers numbers at different flow rates with α = 0.05

radiotracer concentration of the first tank increases with flow rate, as shown in Fig. 29. The activity of the tracer for ADFM and TSFM is computed. These calculations are shown in Table 6. Moreover, the tracer concentration at the outlet was found to be 112018 CPS.
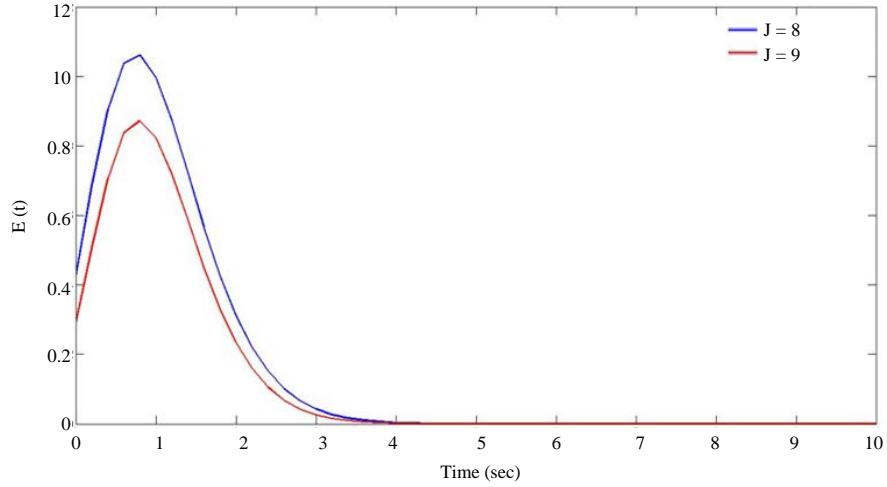
Fig. 26: The radiotracer concentration with time at different number of mixers with $\tau_1 = 201s$, $\tau_2 = 8s$, $Q = 8L/s$, $Q_2 = Q_1$ and $J_2 = 1$
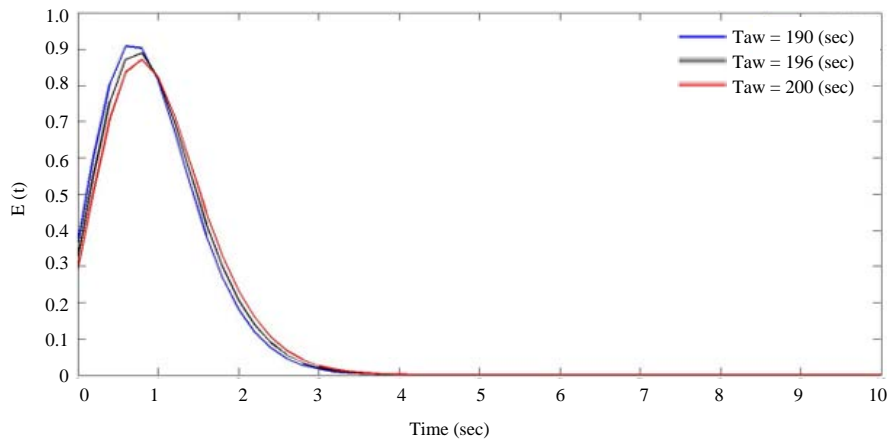

Fig. 27: The radiotracer concentration with time at different mean residence time with $\tau_2 = 8s$, $Q = 8L/s$, $Q_2 = Q_1$ and $J_2 = 1$
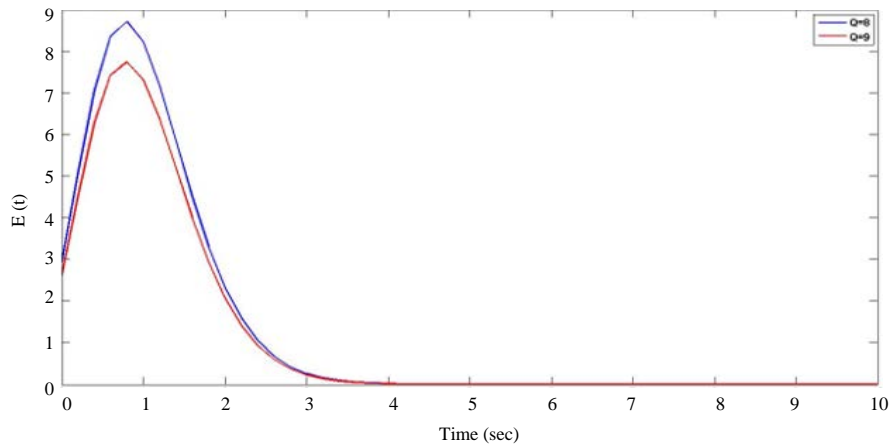

Fig. 28: The radiotracer concentration with time at different flow rates with $\tau_1 = 201s$, $\tau_2 = 8s$, $Q_2 = Q_1$ and $J_2 = 1$
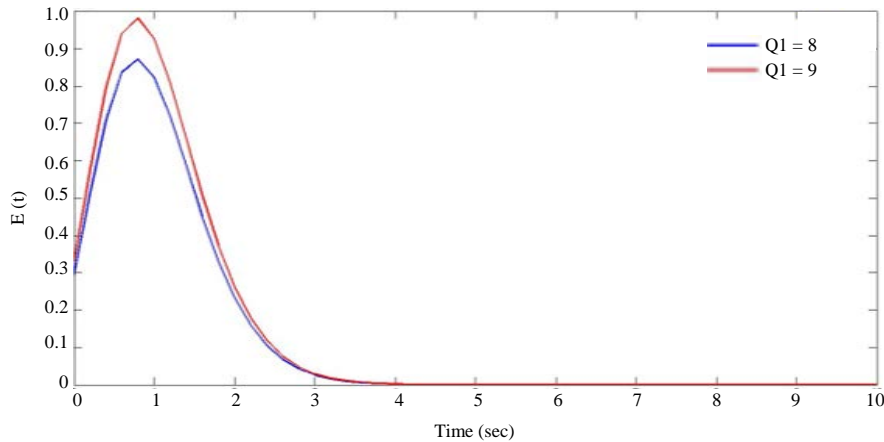
Fig. 29: The radiotracer concentration with time at different first flow rates with $\tau_1 = 201s$, $\tau_2 = 8s$, $Q_2 = Q_1$ and $J_2 = 1$

CONCLUSION

This study discusses the signal pre-processing of the acquired radiation signal for RTD. Radiation signals of ^{99}Mo radiotracer were acquired through system setup. This system begins with a scintillator detector, DAS and a Personal Computer (PC). Different forms of noise are accompanied by RTD radiation signal. Consequently, an algorithm was proposed based on signal processing. This algorithm depends on background correction, baseline restoration, statistical error computation, radioactive decay correction, signal de-noising and dead time correction methods. Background correction was performed using two independent methods. These methods are the minimum value of RTD radiation signal and subtraction method. Then, baseline restoration was performed. Statistical error of RTD radiation signal was computed. However, two different methods are studied for radioactive decay correction. Furthermore, the RTD signal de-noising handling of ^{99}Mo is performed. It is investigated by CWT. The accuracy of the considered algorithm is determined based on statistical measurements of the acquired RTD signal. Moreover, the first moment of the RTD radiation signal is considered. Thus, computation of mean residence time is studied. Consequently, the MRT is simply obtained. The accuracy of the underlined algorithm was evaluated through statistical measurements. The obtained results confirm the effectiveness and importance of RTD measurements for diagnosing process in industrial applications. Moreover, this study focuses on RTD radiation signal modelling and treatment. Therefore, explicit solutions of RTD radiation models are proposed. Also, the implicit solution is introduced. Thus, block diagram modeling of different models of chemical reactors through MATLAB Simulink is implemented. Different effective parameters such as Peclet number, MRT, total volume, flow rate and number of mixers are studied. The radiotracer activity for RTD is experimentally determined for ADFM and TSFM to be

0.1721 and 0.1230 MBq, respectively. Also, the tracer concentration at the output of the experiment was computed and equal to 112018 CPS.

REFERENCES

01. Charlton, J.S. and E.F. Wellman, 1990. Quality improvement in industrial process plants-the role of radioisotopes. Int. J. Radiat. Appl. Instrum. Part A. Applied Radiat. Isot., 41: 1067-1077.
02. Korchi, K.E., R. Alami, A. Saadaoui, S. Mimount and A. Chaouch, 2019. Residence time distribution studies using radiotracers in a lab-scale distillation column: Experiments and modeling. Applied Radiat. Isot., Vol. 154, 10.1016/j.apradiso.2019.108889.
03. Kasban, H., E.H. Ali and H. Arafa, 2017. Diagnosing plant pipeline system performance using radiotracer techniques. Nucl. Eng. Technol., 49: 196-208.
04. Pant, H.J., V.K. Sharma, M.V. Kamudu, S.G. Prakash and S. Krishanamoorthy et al., 2009. Investigation of flow behaviour of coal particles in a pilot-scale fluidized bed gasifier (FBG) using radiotracer technique. Applied Radiat. Isot., 67: 1609-1615.
05. Kasban, H., O. Zahran, H. Arafa, M. El-Kordy, S.M.S. Elaraby and F.E.A. El-Samie, 2010. Laboratory experiments and modeling for industrial radiotracer applications. Applied Radiat. Isotopes, 68: 1049-1056.
06. Yunos, M.A.S.M., S.A. Hussain and S.M. Sipaun, 2019. Industrial radiotracer application in flow rate measurement and flowmeter calibration using 99mTc and 198Au nanoparticles radioisotope. Applied Radiat. Isot., 143: 24-28.
07. Raitoharju, M., Garcia-Fernandez, A.F., R. Hostettler, R. Piche and S. Sarkka, 2020. Gaussian mixture models for signal mapping and positioning. Signal Process., Vol. 168, 10.1016/j.sigpro.2019.107330.

08. Airey, P., C. Hughes, T. Kluss, E. Duran and B. Miller *et al*., 2003. Evolving role of radiotracers in coastal zone studies. Applied Radiat. Isot., 58: 401-406.

09. Kamelnia, E., A. Divsalar, M. Darroudi, P. Yaghmaei and K. Sadri, 2020. Synthesis, 99mTc-radiolabeling and biodistribution of new cellulose nanocrystals from Dorema kopetdaghens. Int. J. Biol. Macromol., 146: 299-310.

10. Pant, H.J., S. Goswami, V.K. Sharma, T. Mukherjee and K. Mukherjee *et al*., 2020. Investigation of flow dynamics of primary coolant in a delay tank of a swimming pool-type nuclear reactor using radiotracer technique. Applied Radiat. Isot., Vol. 156, 10.1016/j.apradiso.2019.108982.

11. Jung, S.H., J. Moon, J.G. Park and J.C. Lim, 2020. Study on visualization of water mixing flows in a digester equipped with a vertical impeller by using radiotracers. Nucl. Eng. Technol., 52: 170-177.

12. Mishra, S.P. and T.B. Singh, 1986. Radiotracer technique in adsorption study-III: Adsorption of phosphate ions on cobalt metal powder. Int. J. Radiat. Appl. Instrum. Part A. Applied Radiat. Isot., 37: 1121-1127.

13. Abdelouahed, H.B., N. Reguigui and N.E. Abbes, 2016. Phosphate slurry RTD-effect of the radiotracer choice. Applied Radiat. Isot., 115: 1-3.

14. Pant, H.J. and V.N. Yelgoankar, 2020. Radiotracer investigations in aniline production reactors. Applied Radiat. Isot., 57: 319-325.

15. Roshani, G.H., R. Hanus, A. Khazaei, M. Zych, E. Nazemi and V. Mosorov, 2018. Density and velocity determination for single-phase flow based on radiotracer technique and neural networks. Flow Meas. Instrum., 61: 9-14.

16. Zniyed, Y., R. Boyer, A.L. de Almeida and G. Favier, 2019. Multidimensional harmonic retrieval based on vandermonde tensor train. Signal Process., 163: 75-86.